Dynamic Resolution Control in a Laser Projection based Stereolithography System

1. Introduction

1.1 Backgrounds and motivations

Additive Manufacturing (AM), also referred to as Solid Freeform Fabrication (SFF) or 3D Printing or Rapid Prototyping, is a class of technologies that can fabricate parts with almost any freeform geometries directly from three-dimensional computer aided models by accumulating material together, usually in a layer by layer manner. In past decades, intensive research attempts have been made to improve the performance of AM systems, in terms of build speed (Ha *et al*., 2008; Pan *et al*., 2012), surface quality (Pan *et al*, 2015; Sun *et al*., 2005; Pan *et al*., 2012), mechanical property of printed parts (Pan *et al*, 2014; Turner *et al*, 2014; Zhao *et al*, 2013), process reliability (Turner *et al*, 2014), etc. This technology finds its applications as a rapid prototyping technology in a wide variety of fields such as architecture, construction, industrial design, automotive industry, medical fields and education (Corner *et al*, 2014; Klahn *et al*, 2013; Chu *et al*, 2010). Despite the advancements, many limitations still exist in AM and hinder its application in fabricating end-use products, including size and resolution limitations, imperfections, limited choices of materials, low through-put, etc. (Huang *et al*., 2013). In this research, we focus on working to overcome one of its primary drawbacks: size and resolution limitations, in stereolithography (SL) related AM processes.

Stereolithography related AM technology has entered the mainstream of 3D printing industry. As of today, various commercial machines have successfully entered the market, typically offering resolutions in the range of 20 μm ~200 μm and build envelope diagonal size of 30 ~ 500 mm. There are two types of stereolithography related AM technologies: laser scanning based, and Digital Light Processing (DLP) projection based technologies. In the early stage, laser beam is used in a SL system to cure liquid resin path by path to form a layer. With the advancement in Micro-Electro-Mechanical Systems (MEMS), the projection based SL process became more popular due to their dynamic mask generation capability. In a projection SL system, a Digital Micromirror Device (DMD) is usually used to pattern the light. A DMD is a Micro-Electro-Mechanical Systems device that enables one to simultaneously control small mirrors that turn on or off a pixel at over 5 KHz. Using this technology, a light projection device can project a dynamically defined mask image onto a resin surface to selectively cure liquid resin into layers of the object. Consequently, the related AM process, Mask Image Projection Stereolithography (MIP-SL), can be much faster than the laser based SL process by simultaneously forming the shape of a whole layer, and can achieve a much higher resolution by having a big number of micro-mirrors and focusing each pixel in a small area. Many research groups demonstrated micro-manufacturing capability with micron or even sub-micron scale resolution in MIP-SL systems (Choi *et al*., 2009; Choi *et al*., 2006; Cheng *et al*., 2009).

Despite the advancement of SL related AM technologies, conflict between the build size and resolution is a historically inherent manufacturing dilemma. In order to achieve higher resolution, a smaller laser beam spot or digital mask with a smaller pixel size is desired, in turn, a smaller build size will be created. Recently stitching based methods have been proposed to solve this dilemma. For example, multiple images were projected in different positions sequentially and stitched to fabricate a large layer (Emami *et al*., 2014). A similar approach was proposed (Lee *et al*., 2015), using a laser beam and a digital micromirror device. In addition, some researchers proposed a combination of laser scanning and projection to realize large area building with micro resolution (Zhou *et al*., 2015; Beke *et al.*, 2014; Benedict, 2015). These pioneering work advances SL related AM technologies by realizing large area and fine details printing simultaneously. Challenges including alignment and bonding strength have been identified. In all those approaches, the pixel size of digital masks or laser dot size and hence the printing resolution is fixed. As a result, the build time is still lengthened and there is no freedom to optimize the combination of resolution, build size and build speed.

Against this background, the thrust of this research is to minimize number of stitches or even avoid stitches to fabricate multi-scale features without sacrificing build speed and part quality. . To achieve this goal, a continuous resolution control approach by using a laser projection technology is investigated in this paper. Instead of the fixed pixel size used in other approaches, the pixel size in the proposed approach could change dynamically and continuously throughout a layer and across layers. Due to this fundamental difference, this new approach is capable of fabricating complex parts with desired fine features in shortest time.

1.2 Novelty and Contributions

A schematic diagram of the MIP-SL process is represented in Fig. 1a. A bulb is usually used as a light source and a DMD chip is used to pattern the light. Optical lenses are used to focus the patterned light onto a liquid resin surface. In such a system, the build area and resolution are generally fixed because of the limited depth of focus. As shown in Fig. 1b, suppose the build area is 250 mm in x direction and there are 1000 pixels along x direction, the smallest feature that can be built would be constrained by the pixel size, which is 250 μm in this example. In order to fabricate features smaller than 250 μm, the optics in the system needs to be modified to focus the light into a smaller image. The build area will be reduced greatly as a result.

Current approaches to building large area with small features are based on projecting multiple images and stitching these areas together, as illustrated in Figure 2 (a) and 2 (b). To build a large layer, the projection unit moves along X and Y directions to project images in Pos 1~9 sequentially, as shown in Figure 2(b). In these approaches, the number of stitched images to form a certain layer is determined by the resolution. With a higher resolution, more stitches and longer build time will be resulted.

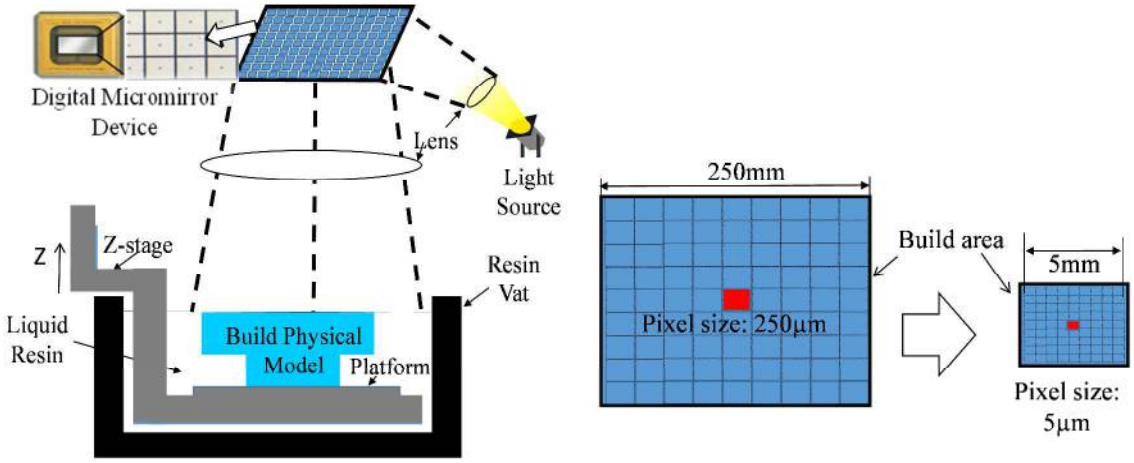

(a) (b)

Figure 1. (a) Schematic illustration of conventional MIP-SL systems (b) Tradeoff between feature size and curing area in conventional MIP-SL

In contrast, a laser projector is used in the proposed approach, as shown in Figure 2 (c). The projection unit moves along Z-axis and the resulted projection image is always in focus. Accordingly, the resolution could be tuned dynamically in a certain range by moving the projector along Z-axis. As a result, the number of stitches could be optimized and therefore the build time could be much shorter than any current approaches. As shown in Figure 2 (d), suppose that there is no small feature in Pos 1, Pos 2 contains small features and Pos 3 contains even smaller features, three images with low, median, and high resolutions could be planned to cure Pos 1, Pos 2 and Pos 3 sequentially to form the entire layer. Comparing to the conventional approach in Figure 2 (b), which needs nine stitches, the build time of the new approach would be much shorter and the part quality would probably be better due to less aligning and stitching operations.

This dynamic resolution control approach is presented in the following sections. Section 2 presents an overview of the system design along with a flowchart explaining the working of the system. A mask image planning for dynamic resolution control is presented in Section 3, followed with a parametric dependence quantification process investigated in Section 4. Multiple test cases are demonstrated and discussed in Section 5. Finally, conclusions are made in Section 6.

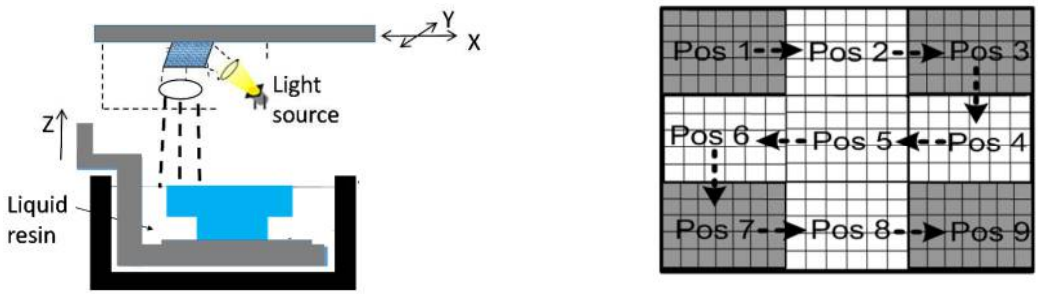

(a) Conventional approach: hardware setup (b) Single resolution image stitching

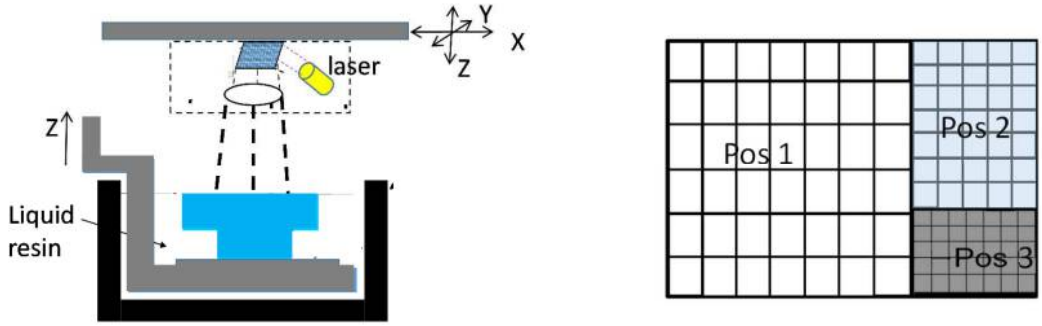

(c) Proposed approach: hardware setup (d) Proposed approach: multiple resolution image stitching

Figure 2. A comparison of conventional stitching approaches and the proposed approach: (a) Illustration of approaches based on a light source that is movable along X and Y axes; (b) Curing and stitching of pieces with a signle resolution; (c) Illustration of proposed approach based on a laser projector which is movable along X, Y and Z axes; (d) Curing and stitching of pieces with multiple resolutions.

2. Overview of the Laser Projection based SL System

Instead of a bulb, a pixel scanning based laser projector is used as a projection light source in our system. The laser projector has unique properties including focus free operation, capability to produce dynamic mask image irrespective of any surface (flat or curved) as shown in Fig. 3. In addition, the compact size that makes it easy to be adopted and integrated into the additive manufacturing system. These unique characteristics of laser projector eventually provide a distinct capability to change the projection image size and resolution easily.

(a) (b)

Figure 3. Unique properties of the pixel scanning based laser projector: (a) Stays focus when changing focal length; (b) Project on any shape surface

The laser projector is composed of an integrated photonics module, laser drive electronics and a silicon bi-axial scanning mirror. The integrated photonics module consists of three lasers and opto-mechanical components to perform three functions: beam shaping and focusing, beam combining and beam coupling. The laser beam is transformed into a focused spot that matches the resolution of the scanner. In addition, the beam would not exceed the size of a pixel. The integrated photonics module coupled with laser drive electronics and the bi-axial scanning mirror to draw a two-dimensional image at the image plane, in a pixel-by-pixel fashion. Because of the scanned single pixel design, the power efficiency is maximized since the lasers are only on at the level needed for each pixel. In addition, compared to the projectors based on DMD chips, the contrast is inherently high since the lasers are completely off for black pixels. To avoid optical

distortions and enable brightness uniformity, a Virtual Pixel Synthesis (VPS) engine was adopted in the laser projector design. The VPS uses a high-resolution interpolation to map the input pixels onto a high-resolution virtual coordinate grid. Through an adaptive laser drive system that uses closed-loop control, the spot size grows at a rate matched to the growth of a single pixel. Furthermore, because the bi-axial scanner replaces projection optics, the projected image remains in focus at any projection distance (Davis *et al*., 2008; Sprague *et al*., 2008).

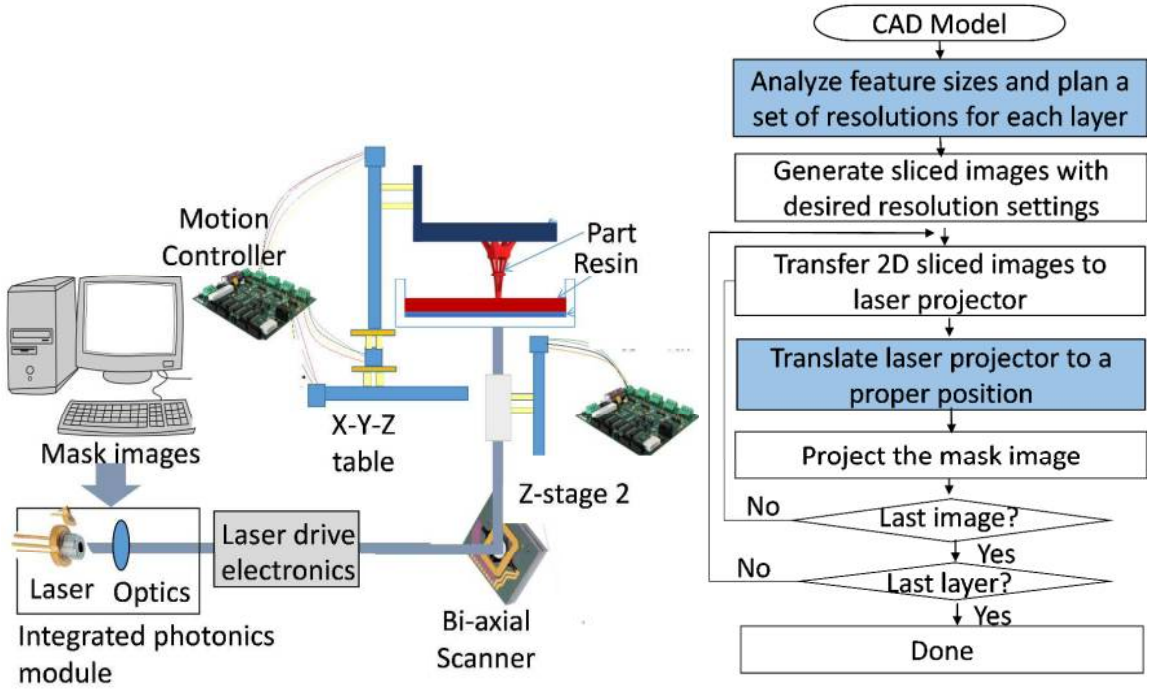

(a) (b)

Figure 4. (a) A laser projection based SL system with dynamic resolution control (b) Flowchart of the working of the system

The Laser Projection based SL system design is shown in Fig. 4 (a) and the flowchart in Fig. 4 (b) explains the working of the entire system. In this study, the resolution setting is denoted as R#, meaning the resolution is # μm/pixel. Similar to the conventional approach, we start from a CAD model. However, instead of slicing the STL file with a certain predefined resolution setting, we first analyze feature sizes, and then plan a single or multiple mask images for each layer. After that, one or multiple mask images will be generated by slicing each layer with the planned resolution settings. These mask images are then transferred to the laser projector. The laser projector moves to the proper Z level to gain the desired image resolution, and then project the image to build features with the desired resolution. Therefore, in this dynamic resolution control manufacturing process the mask image planning and projection location are the most important. Correspondingly, two fundamental research questions need to be answered:

Q1. How to determine a proper set of resolutions for each layer to achieve best part quality and fastest build speed.

Q2. How to move projector to the proper position to gain the required resolution.

Question 1 will be answered in Section 3 by exploring an image processing algorithm to filter features with different resolution requirements. Question 2 will be investigated in Section 4 by quantifying the parametric dependence of resolution and build size on manufacturing process parameters.

3. Mask Image Planning in Dynamic Resolution Control Approach

It is very essential to answer the first question about how to determine proper resolution for each layer to obtain best part quality. In this study, a single Layered Depth Image (LDI) algorithm is utilized to determine the proper set of resolutions for each layer. LDI is generally used for 2-dimensional images that can be extended further to Layered Depth-Normal Images (LDNI) (Wang *et al*., 2010). In the following sections, for easy understanding, we use "micro feature" or "micro image" to denote an area that has to use a high resolution, and "macro feature" or "macro image" to denote an area that could use a low resolution.

An example is shown in Fig. 5. It illustrates a simple sliced binary image for a single layer that contains micro feature in a large area. We segmented the micro features from the macro part to build these small features with higher resolution in order to highlight its intricate details. Let V comprises of the entire image having i pixels along X-direction and j pixels along Y-direction. This can be represented as $(X_i, Y_j) \in V$ for a single layer that can be extended to the 3rd dimension identifying the K^{th} sliced layer. Thus the overall equation can be represented as $(X_i, Y_j) \in V_{Layer\_K.}$ Originally, the image is sliced by using the desired resolution for fabricating the smallest feature in the model, for example, R41 in Figure 5. Rays are transmitted along each row pixel first and then each column pixel to filter small features from the large area which does not require high resolution fabrication. We consider each row as a separate image and run the loop. When the ray identifies a pixel that has its neighboring pixel of different intensity, it shall be marked as the boundary of the object.

In the following example, a sectional part is highlighted to show the working of the process. The system identifies the object pixel and marks the boundary pixel at the respective position as $X_{i,n}$, where i is the pixel location and n is the number of times that the pixel color changes in each row or column. The value of n starts from 0 and changes to 1 immediately when it finds the 1st boundary pixel and then proceeds with an increment when it encounters pixel color changes. Thus, the next boundary will have $X_{i+p,n+1}$. The distance between any two boundaries of an object can be generalized as $d|X_{i+p,n\_even} - X_{i,(n\_even)-1}|$, except when n is 0. A threshold feature size, defined by a variable T, is set based on the resolution. Based on experience, T is set as seven times of the resolution in our study. For example, if the distance between two neighboring boundary pixels exceeds a threshold T of 427 microns, the area between these two boundary

pixels will be counted as macro sized feature that will be fabricated using resolution R61, whereas if the distance between the boundary pixels is less than the threshold it will be counted as the micro-scale feature which needs to be fabricated by using higher resolutions.

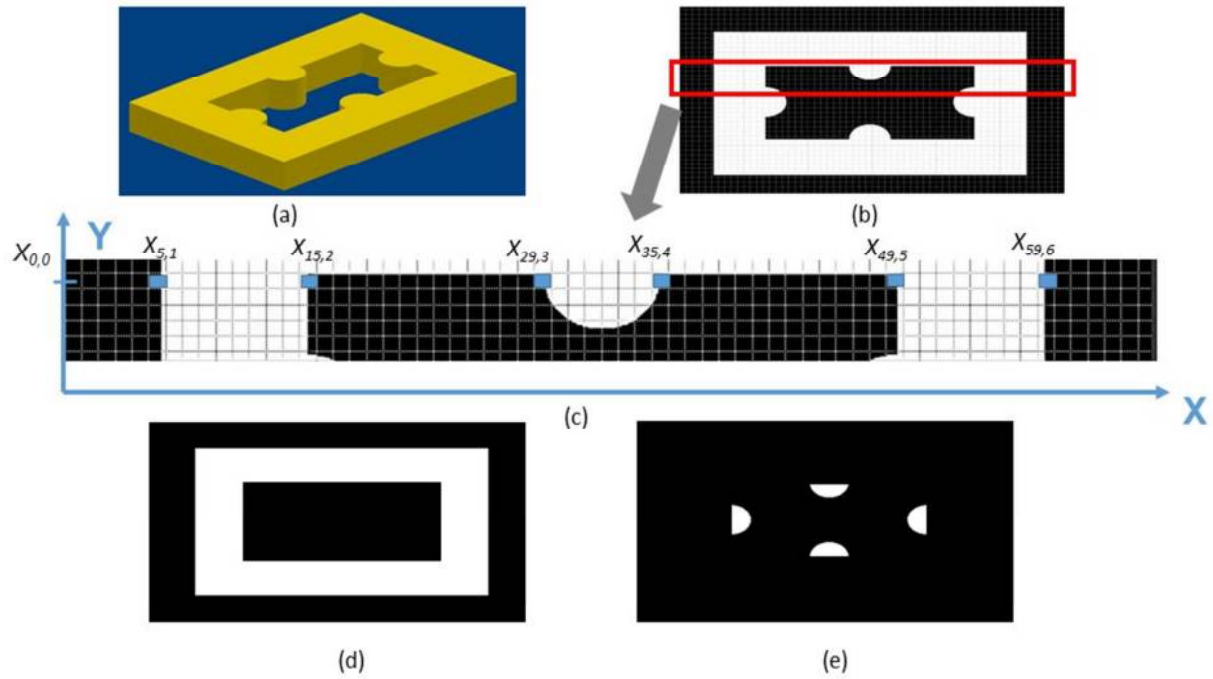

Figure 5. Example Model (a) STL model; (b) Transfer rays along rows and columns of a binary sliced layered image; (c) Sectional view highlighting object and boundary detection; (d) Macro image; (e) Micro image

For example, in the sectional image in Fig. 5 (b), the ray transmitted along the row starts with n as 0 and then ends with n as 6, thus the row has 6 boundaries and 3 objects. It is identified that the $d|X_{15,2} - X_{5,1}|$ and $d|X_{59,6} - X_{49,5}|$ is greater than the threshold T, thus identified as macro scale features and will be cured by an image of R61. On the contrary, the other object is micro scale features since the $d|\ X_{35,4} - X_{29,3}|$ is less than T and it will be cured by an image of R41. After identifying the micro-scale features, it will set all the micro pixel object area to zero, the loop for all the rows will be run to generate a new image. For better efficiency, we then run this loop for all the columns on the new image and again the identified micro objects are set zero forming a modified image. The modified image thus obtained is the macro image and subtracting this modified image from the initial image will give out a micro image. Then the macro image is used for fabricating the related part by using R61. The micro features separated from the original sliced image, a higher resolution R61-△ (denoting a resolution of 61-△ microns per pixel) is used to regenerate an image for the micro features. A value of 20 is used for △ in the example. Then the regenerated image is used as the input image and is processed the same way to determine a proper resolution for it.

Image processing process for the example in Figure 5:

INPUT

A binary image sliced by using R41, V of K^{th} layer

T= 61;

OUTPUT

1. Macro image with resolution R61

2. Micro image with resolution R41

STEPS

1. Transfer rays from Y_j till Y_{j+w}, where j=0 → w and w = number of pixels along Y-axis
2. For each row find boundary pixel, $X_{i,n,}$ where i=0 → v and v= number of pixels along X-axis and n= change in pixel intensity
3. If $d|X_{i+p,n\_even} - X_{i,(n\_even)-1}| \geq T$, macro image else micro-image
4. If $d|X_{i+p,n\_even} - X_{i,(n\_even)-1}| < T$, set $d|X_{i+p,n\_even} - X_{i,(n\_even)-1}| = 0$
5. New image as V_row
6. Repeat above steps for column rays on V_row
7. Store the modified image V_mac
8. V_mic =V - V_mac

RESULT

V_mac as macro image, which will be used to fabricate large features of that layer using resolution R61

V_mic as micro image, which will be used to fabricate small features of that layer using resolution R41

4. Parametric Dependence Quantification

After obtaining images with the desired resolutions for each layer using the above approach, the next thing is to move the laser projector to the corresponding position to fabricate that layer with the generated mask images. The dependence of pixel size and build size on the focal length is first quantified. By moving the laser projector up and down, exposure on the liquid resin surface would have changing pixel size and exposure size. More specifically if the laser projector is moved away from the platform the pixel size increases which means lower resolution but bigger build area. For example, the micro scale structures could be segmented and fabricated with a small focal length and hence higher resolution, while the meso-scale structures in the model could be fabricated with a bigger focal length and hence larger curing area. The following section investigates the relationship between pixel size and build size on the focal length.

4.1 Dependence of Build Area and Planar Resolution on Focal Length

Due to the laser property of producing focus free masks irrespective of any focal distance, it provides a wide variety of resolution depending upon its distance from the projection plane. Thus, a process planning approach is essential for determining the position of the projector to obtain the required resolution for each layer. First, experiments were performed to calibrate the

working range of focal length. As shown in Fig. 6, the projector provides a good flexibility with a focal length ranging from 20.0 mm to 70.0 mm, leading to a build area ranging from 31.0 mm to 73.0 mm along X-axis, 17.54 mm to 41.32 mm along Y-axis, and a resolution from 36.55 micron/pixel to 86.08 micron/pixel. Because of the straight projection light path, both the resolution and build area are related to the focal length linearly (Davis *et al.,* 2008). To validate the linear relationship, the build sizes and resolution at the middle point of the working range, that is, f=45 mm, were measured. The relationship of focal length f (mm) and building sizes along X and Y-axis are denoted by the blue dashed line and orange round dotted line respectively. The linear relationship could be formulated as the following:

$A\_x = 0.8 \times f + 14.1333$ A_x : build size along X-axis

$A\_y = 0.4756 \times f + 7.9913$ A_y : build size along Y-axis

The relationship of focal length f (mm) and the resolution R (micron/pixel) is plotted as the red line in Figure 6 can be described by:

$R = 0.9906 \times f + 16.6597$

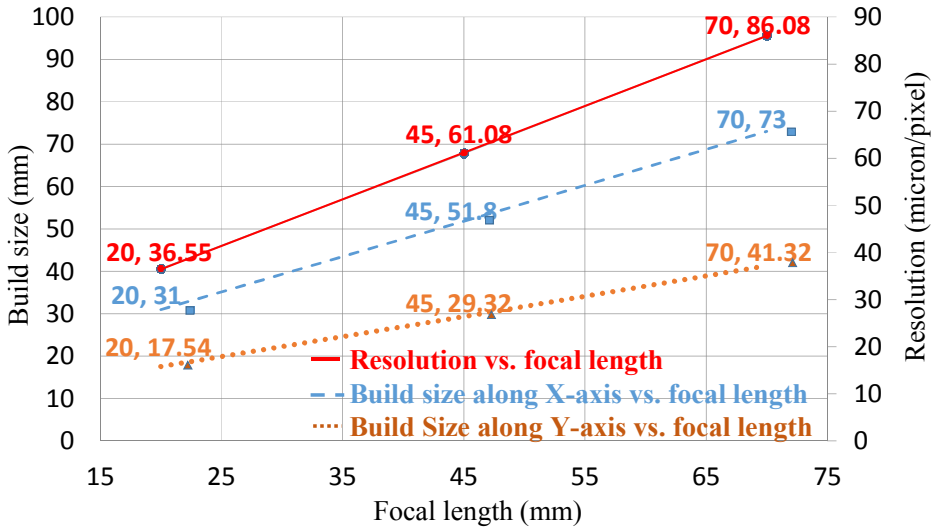

Figure 6. Graphical relationship between focal length, build area and planar resolution

From the above equations, it is obvious that the focal distance between the laser projector and projection plane should be small to produce fine features and conversely for the development of parts with large features the focal distance should be larger. Given a desired resolution, the projector could be moved to the corresponding position. For the fabrication of one layer with large area but small features, the mask image could be segmented into multiple images for multiple curing with different projector positions.

4.2 Dependence of Vertical Resolution on Focal Length

Experiments were conducted for further analysis of the vertical resolution by measuring cure depth (C_d). In the experiment, the laser projector produced a mask at 20.0 mm, 30.0 mm, 40.0 mm, 50.0 mm, 60.0 mm and 70.0 mm focal lengths with each having a set of exposure time of 200 s, 300 s, 400 s, 500 s and 600 s. A commercial resin "Acryl R5" from Envisiontec containing 2% photoinitiator was used for the following set of experiments. Four replications were performed to measure the cure depth for each exposure. Resin parameters such as penetration depth D_p and critical exposure E_c can be obtained from the Beer-Lambert formula provided in equation below (Jacobs; 1992):

$$C_d = D_p \times \ln\left(\frac{E_{max}}{E_c}\right) \quad (1)$$

Also, the values of D_p and E_c can be verified from the graph below. The graph shows the relation between cure depth and exposure energy per unit area on the resin surface. The results indicate the cure depth is linearly proportional to the natural logarithm of the energy per unit area. Theoretically, the slope of the line is its penetration depth D_p and E_c is the energy when cure depth is 0, but this does not indicate the gel point of the resin (Gibson *et al.,* 2010). It is observed from the graph that the value of D_p is 0.266 mm whereas E_c is 23.46 mJ/cm^2.

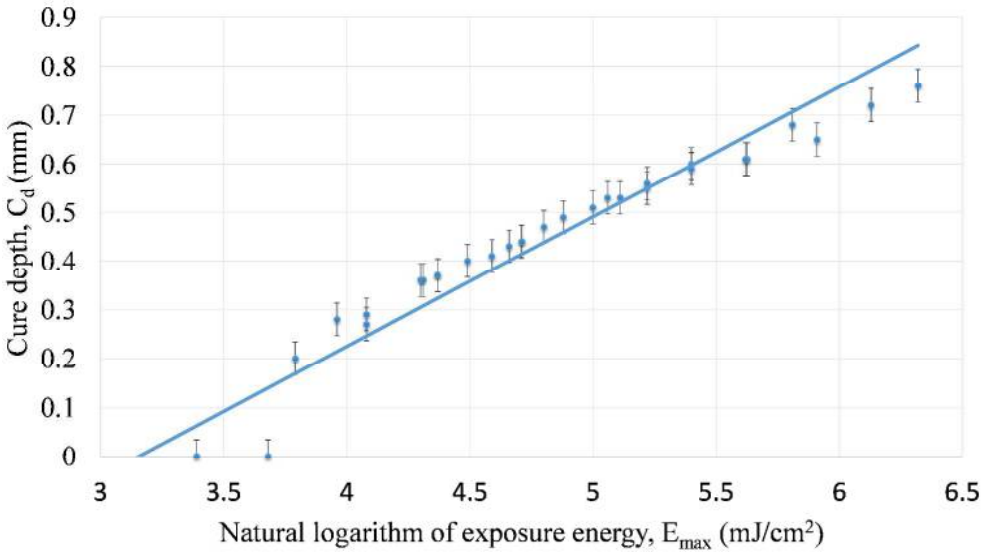

Figure 7. Graphical relationship between exposure energy and cure depth

By further extending Beer Lambert equation, the relationship between the cure depth C_d and focal length f can be derived using Equation (1) as:

$$C_d = D_p \times \ln\left(\frac{P_{max} \times t_c}{A \times E_c}\right) \quad (2)$$

where P_{max} is the laser power, t_c is the exposure time, A is the build area.

Since the build area A is directly proportional to the focal length f, Equation (2) can be represented as follows:

$$C_d = D_p \times \ln\left(\frac{P_{max} \times t_c}{K \times f \times E_c}\right) \quad (3)$$

where $K = A/f$. Given a specific focal length and exposure time, all the variables in Equation (3) could be approximated as constants, leading to the following equation:

$$C_d = K_{constant} - D_p \times \ln(f) \quad (4)$$

where $K_{constant}$ is $D_p \times ln(\frac{P_{max} \times t_c}{K \times E_c})$. The linear relationship was validated by experimental results as shown in Figure 8. In the experiments, an overhanging layer was cured by projecting a mask image with an exposure time ranging from 200 sec to 600 sec, and a focal length ranging from 2.9 mm to 4.18 mm. The thickness of the cured layer was measured and recorded as the cure depth associated to the exposure time and focal length. The experimental results are plotted in Figure 8. The linear relationship of cured depth and focal length in Equation (4) was verified.

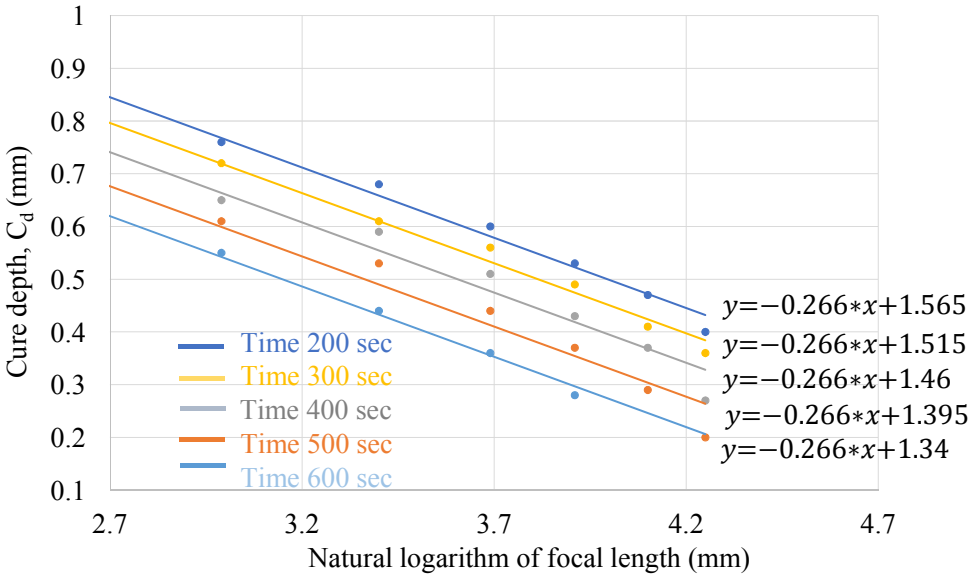

Figure 8. Linear relationship between focal length and cure depth

5. Experimental Setup

5.1 Hardware System

A prototype system has been built to verify the developed process. The hardware setup of the laser projection based SL system is shown in Fig. 9a. In the designed system, an off-the-shelf laser projector (SHOWWX+) from MicroVision was used. It has a native resolution of 848 x 480 while it supports other resolutions like 800 x 400 and 640 x 480. The projection image is always in focus with a projection distance from 6" to 100". Correspondingly, its image size could as big as 100 inch. Due to this unique free focus property, it can move along Z-axis rapidly, thus changing resolution dynamically and continuously. Various projection settings, including optic lens, aspect ratio, key stone rectification, brightness, and contrast were adjusted to achieve a

sharp projection image on the designed projection plane and within the focal length designed in this project. Two precise linear stages from Velmex (Bloomfield, NY) are used as the elevator for driving the platform in the Z axis, and the elevator for driving the laser projector in the Z axis. As this is a prototype testbed to show the dynamic resolution control approach, X and Y stages for moving the platform around are not incorporated in the prototype. A high performance 4-axis motion control board with 28 bidirectional I/O pins from Dynomotion Inc. (Calabasas, CA) is used for driving the linear stages. A flat and clear glass Petri dish is used as resin tank. A PDMS film (Sylgard 184, Dow Corning) is coated on the glass dish.

5.2 Software System

A mask planning testbed has been developed using the C++ language with Microsoft Visual C++ compiler. The testbed integrates the geometry slicing with varied resolution settings, and the motion controlling of Z-stage1 and Z-stage 2. The software also synchronizes the image projection with the platform and projector movements. The graphical user interface of the developed software system is shown in Fig. 9 (b).

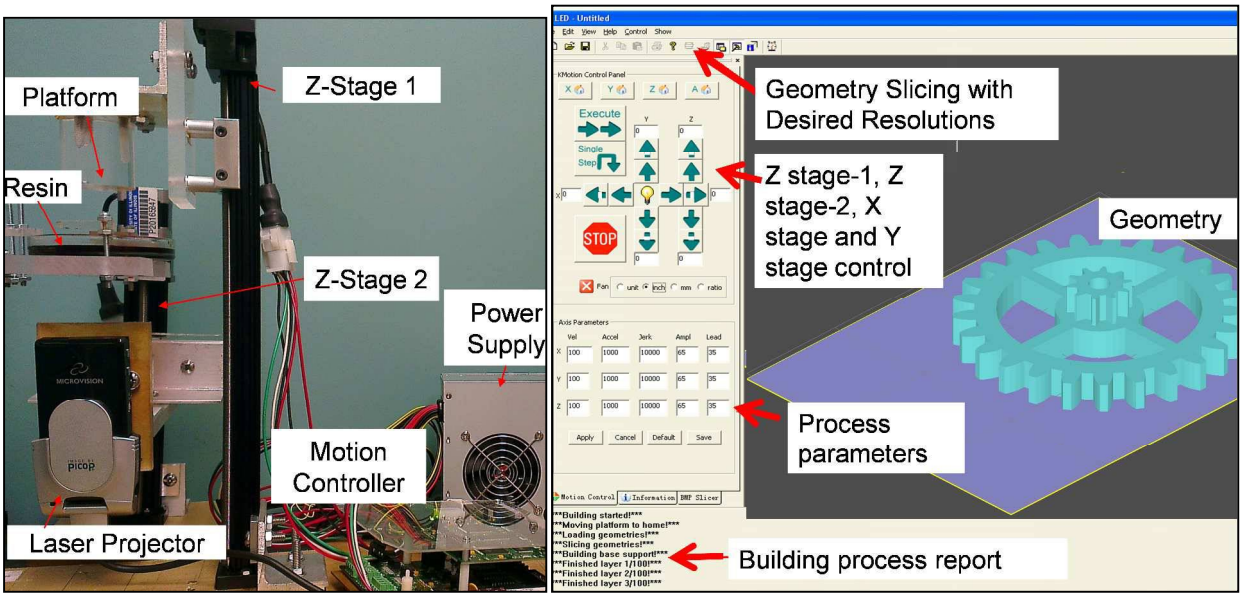

(a) (b)

Figure 9. (a) The prototype hardware system for the laser projection SL process with dynamic resolution control (b) GUI of the control software

5.3 Materials

A commercial resin, "Acryl R5" from EnvisionTEC Inc. (Ferndale, MI), was used in testing the developed dynamic resolution fabrication process. Due to the low brightness of the projector (15 lumens), for the layer thickness of 0.09 mm and a resolution of 81 micron/pixel, the exposure time for liquid resin based on our projection system is set at 70 s. For smaller layer thickness, shorter exposure will be used.

6. Experimental Results and Discussion

To verify the efficacy of the approach, a testbed was developed and models with multiple resolutions, varied sizes were fabricated. These 3D STL models were initially sliced layer by layer into 2D images and projected through a portable laser projector. The unique feature of these experiments was tuning the focal length dynamically to achieve dynamic resolution during building processes. This resulted in providing flexibility to fabricate parts with changing feature sizes and cross section areas in a single building task.

6.1 Large Area Fabrication with Resolution R81

The manufacturing capability of fabricating parts with large layer areas was tested and verified by fabricating a spur gear. The CAD model and fabricated result are shown in Fig. 10. After analyzing this model using our image processing approach, it was found that the part can be fabricated with one resolution. A resolution of 81 micron/pixel was adopted which is good enough to produce all details of this gear model. Based on the resolution and focal length relationship, the laser projector's focal length was kept at 65 mm to obtain the desired resolution.

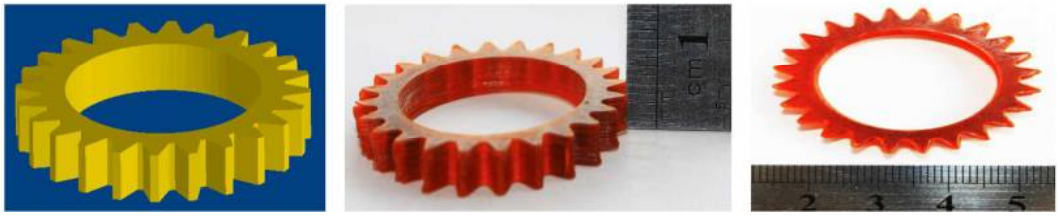

(a) (b) (c)

Figure 10. Gear- (a) Isometric view of STL Model; (b) Isometric view and (c) Top View of Built Part

This fabricated model constituted of 50 layers in total, including 7 base layers with a layer thickness of 90 microns. Initial exposure time for the base layer was 600 seconds per layer whereas for the subsequent layer it was 70 seconds each.

6.2 Small Area Fabrication with Resolution R30

The system showed appropriate results for large area fabrication. The same experimental setup was adopted to test the limits of resolution and efficacy of small area fabrication. The CAD model as demonstrated in Fig. 11 (a) is a hollow ball with nine circular cuts on its circumference. Four symmetric bigger circular cuts along the center whereas slightly above it includes four circular cuts of slightly smaller diameter. Lastly, the top portion is drilled to form the smallest circle. The image processing analysis showed that a single resolution, 30 μm/pixel works for fabricating the whole part with desired accuracy while a shortest build time. Thus, the focal length was fixed at 13.5 mm to give a 30 μm/pixel resolution for building all layers.

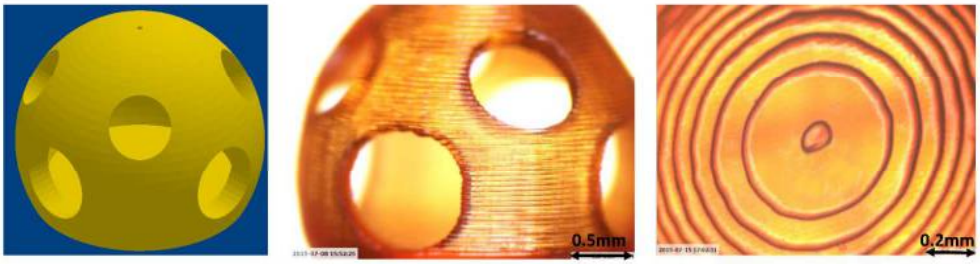

(a) (b) (c)

Figure 11. Hollow ball test case: (a) STL model; (b) Built part; (c) A microscopic image of the top

The fabricated part, thus formed was 2.8 mm in diameter and 2.65 mm in height with bigger and smaller circular cuts of diameter 800 μm and 600 μm respectively. Also, the top circular portion had a diameter of 70 μm. The Fig. 11 (b) and 11 (c) are microscopic images of the isometric and top view of the part respectively. The entire structure was comprised of 63 layers including 7 base layers. Each layer corresponds to a thickness of 43 microns. Due to the reduced focal length, the exposure time for base layers and subsequent layers were set as 200 seconds and 30 seconds respectively.

6.3 Multi-Scale Fabrication with Resolutions R41, R61 and R81

The system successfully fabricated parts with micro and macro scale features separately. The following test case is conducted to verify the manufacturing capability of building multi scale features in a single building task. For this purpose a gear set with concentric center was designed as shown in Fig. 12 (a). With our dynamic resolution control method, after applying the image processing algorithm, we identified that for the bottom gear, a pixel size of 81 micron is good enough to give the desired accuracy and build size. For the top gear, since its feature is much smaller, a smaller pixel size, 41 micron, is desired to fabricate the features precisely. After setting up different resolutions for layers, we could assign the corresponding projector position. According to the parametric dependence, the focal length was obtained as 65 mm and 25 mm for the bottom and top gear respectively.

(a) (b) (c)

Figure 12. Gear test case: (a) STL model; (b) Built part; (c) A microscopic image of the top gear

The fabricated part constituted 39 layers including 7 base layers with a layer thickness of 90 micron. The 7 base layers were cured for 600 seconds and the subsequent 13 layers were cured for 70 seconds whereas the last 19 layers were cured for 35 s. The bottom gear diameter

comprised of 30.0 mm whereas the top gear diameter comprised of 5.00 mm with an overall depth of 3.8 mm.

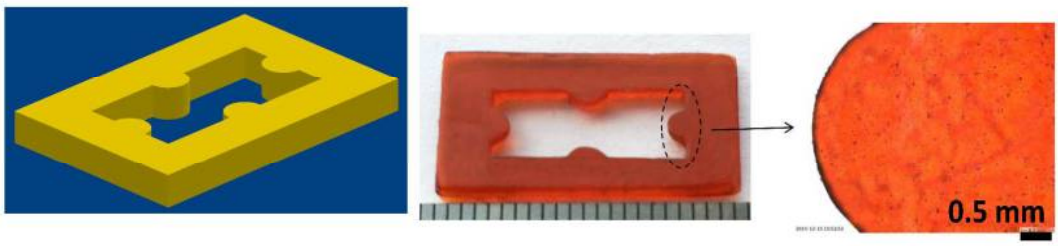

(a) (b) (c)

Figure 13. Frame test case: (a) STL model; (b) the build part; (c) a microscopic image

The example showed in Figure 5 was also tested. As discussed in Section 3, each layer was fabricated by using R61 and R41. The cross section was segmented to two portions, the four teeth, and the rectangular frame. The projector first moves to 24.6 mm level to cure the teeth with the micro image, which has a resolution of R41. Then it moves to 44.7 mm level to cure the rectangular frame with the macro image, which has a resolution of R61. An entire layer was then be formed by stitching these two areas. A 30s exposure time was used for both micro image and macro image exposures. Figure 13 shows the fabricated part and microscopic image of the small feature.

6.4 Continuous Resolution Control Fabrication with R41-R61

The first two test cases in Section 6.1 and 6.2 demonstrate the capability of our approach on fabricating parts with different resolutions. Section 6.3 verifies the effectiveness and efficiency of our approach on fabricating a part with two different resolution settings in one build. Furthermore, another test case is conducted to demonstrate the system capability in continuously changing the resolution for each layer. The STL file shown below in Fig. 14 (a) consists of a triangular structure with a circular hole drilled through its center. The two sides of the triangle are drafted by an angle of 55 degree. Since the layer by layer sectional area of the part reduced continuously, the projector's focal length was also changed from 45.0 mm to 25.0 mm ultimately improving the resolution by 0.34 micron/pixel for each layer. The focal length was controlled by synchronizing its motion with the platform.

The model comprised of 59 layers in total with each layer thickness corresponding to 76 micron. The base layer of the model was fabricated with an exposure time of 300 seconds whereas the subsequent layers were cured for 30 seconds each. The isometric view along with part dimension is shown below in Fig. 14(b) and 14(c). The side of the triangle is measured to be 18.0 mm whereas the circular hole has a diameter of 5.0 mm. The top tilted edge is 9 mm long while the part thickness are measured to be 4.5 mm.

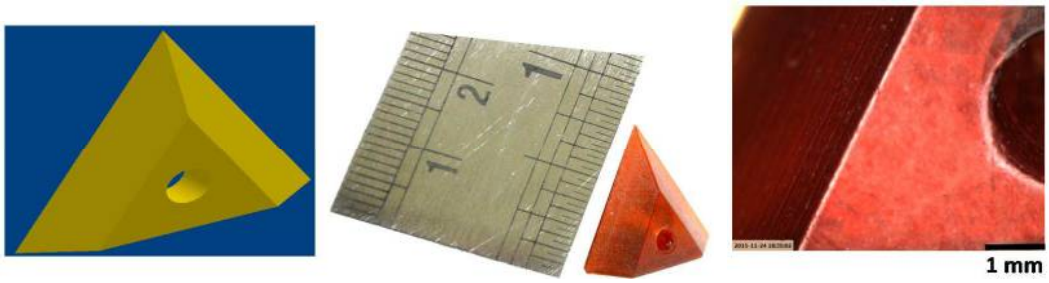

(a) (b) (c)

Figure 14. Titled edges triangular surface: (a) STL model; (b) built part; (c) Microscopic image of the fabricated layers

6.5 Building Performance Statistics

Table 1 shows the effectiveness and efficiency of this approach on fabricating parts with different layer areas and feature sizes efficiently through changing resolutions dynamically and even continuously for each layer. In the table, the build time was also compared with the time needed by using the conventional stitching approaches that use a single resolution. The test cases demonstrated the unique advantages of the dynamic resolution control approach on building large sized objects with small features without sacrificing the build speed.

Table 1. Statistics of all multi-resolution test cases

Model	**Gear- Fig. 12**	**Frame- Fig. 13**	**Triangle- Fig. 14**
Type	***Multi-scale area, multi-resolution in one build***	***Constant area, multi-resolution in one layer***	***Changing area, changing resolution in one build***
X-Y dimension (mm)	30.0 x 30.0	22.0 x 11.0	18.0 x 16.0
Depth (mm)	3.5	1.9	4.5
Layer thickness (microns)	90	76	76
Build time (min)	45	24	30
Build time using conventional methods (min)	180	72	70
Resolution Settings(micron/pixel)	81 (layer 1-20) , 41 (layer 21-39)	61 (outer part), 41(inner part)	41~61

7. Conclusion

A novel mask image projection based stereolithography (MIP-SL) system has been developed to achieve dynamic resolution control. Compared to conventional MIP-SL systems that stitch multiple images with a single resolution to form a large layer, the developed approach is based on fabricating layers with changing resolution. The number of stitches can be therefore minimized. As a result, the build speed could be optimized and the part quality would be probably better. The light source in our design includes a compact laser projector that was mounted on a z-stage, which resulted in changing focal length and in turn projection area and resolution. To facilitate the mask image planning in dynamic resolution control approach, an image segmentation approach has been developed to separate micro features from a sliced image. Parametric dependence of resolution and build size on focal length have been calibrated and modeled. The effectiveness and efficiency of the system has been verified with multiple test cases with various surface areas, feature sizes and structures.

References

Ha, Y.M., Choi, J.W. and Lee, S.H., (2008), "Mass production of 3-D microstructures using projection microstereolithography" Journal of Mechanical Science and Technology, Vol. 22, No. 3, pp. 514-521.

Pan, Y., Zhou, C. and Chen, Y., (2012), "A Fast Mask Projection Stereolithography Process for Fabricating Digital Models in Minutes" Journal of Manufacturing Science and Engineering, Vol. 134, No. 5, pp. 051011.

Pan, Y. and Chen, Y., (2015), "Smooth Surface Fabrication based on Controlled Meniscus and Cure Depth in Micro-Stereolithography", Journal of Micro and Nano-Manufacturing, Vol. 3, No. 3, pp. 031001.

Sun, C., Fang, N., Wu, D.M. and Zhang, X (2005) "Projection micro-stereolithography using digital micro-mirror dynamic mask" Sensors and Actuators A:Physical, Vol. 121, No.1, pp. 113-120.
Pan, Y., Zhao, X., Zhou, C. and Chen, Y., (2012), "Smooth surface fabrication in mask projection based stereolithography" Journal of Manufacturing Processes, Vol. 14, No. 4, pp. 460-470.

Pan, Y., Zhou, C., Chen, Y. and Partanen, J., (2014), "Multitool and Multi-Axis Computer Numerically Controlled Accumulation for Fabricating Conformal Features on Curved Surfaces" Journal of Manufacturing Science and Engineering-Transactions of the ASME, Vol. 136, No.3, pp. 031007.

Turner, B., Strong, R. and Gold, S., (2014), "A review of melt extrusion additive manufacturing processes: I. Process design and modeling" Rapid Prototyping Journal, Vol. 20, No. 3, pp. 192-204.

Zhao, X., Pan, Y., Zhou, C., Chen, Y. and Wang, C.C., (2013), "An integrated CNC accumulation system for automatic building-around-inserts" Journal of Manufacturing Processes, Vol. 15, No. 4, pp. 432-443.

Conner, B.P., Manogharan, G.P., Martof, A.N., Rodomsky, L.M., Rodomsky, C.M., Jordan, D.C. and Limperos, J.W., (2014), "Making sense of 3D printing: Creating a map of additive manufacturing products and services" Additive Manufacturing, Vol. 1, pp. 64-76.

Klahn, C., Bechmann, F., Hofmann, S., Dinkel, M. and Emmelmann, C., (2013), "Laser additive manufacturing of gas permeable structures", Physics Procedia 41, pp. 873-880.

Chu, J., Engelbrecht, S., Graf, G. and Rosen, D.W., et al., (2010), "A comparison of synthesis methods for cellular structures with application to additive manufacturing" Rapid Prototyping Journal, Vol. 16, No. 4, pp. 275–283.

Huang, S.H., Liu, P., Mokasdar, A. and Hou, L., (2013), "Additive manufacturing and its societal impact: a literature review" The International Journal of Advanced Manufacturing Technology. Vol. 67, No. 5-8, pp. 1191-1203.

Choi, J.W., Wicker, R., Lee, S.H., Choi, K.H., Ha, C.S. and Chung, I., (2009), "Fabrication of 3D biocompatible/biodegradable micro-scaffolds using dynamic mask projection microstereolithography" Journal of Materials Processing Technology, Vol. 209, No. 15, pp. 5494-5503.

Choi, J.W., Ha, Y.M., Lee, S.H. and Choi, K.H., (2006), "Design of microstereolithography system based on dynamic image projection for fabrication of three-dimensional microstructures" Journal of mechanical science and technology, Vol. 20, No. 12, pp. 2094-2104.

Cheng, Y. L. and Lee, M. L., (2009), "Development of dynamic masking rapid prototyping system for application in tissue engineering" Rapid Prototyping Journal, Vol. 15, No. 1, pp. 29-41.

Emami, M.M., Barazandeh, F. and Yaghmaie, F., (2014), "Scanning-projection based stereolithography: Method and structure." Sensors and Actuators A: Physical 218, pp. 116-124.

Lee, M.P., Cooper, G.J., Hinkley, T., Gibson, G.M., Padgett, M.J. and Cronin, L., (2015), "Development of a 3D printer using scanning projection stereolithography." Scientific reports 5.

Zhou, C., Ye, H. and Zhang, F., (2015), "A Novel Low-Cost Stereolithography Process Based on Vector Scanning and Mask Projection for High-Accuracy, High-Speed, High-Throughput, and Large-Area Fabrication." Journal of Computing and Information Science in Engineering 15.1: 011003.

Beke, S., Farkas, B., Romano, I. and Brandi, F., (2014). "3D scaffold fabrication by mask projection excimer laser stereolithography. " Optical Materials Express, 4(10), pp.2032-2041.

Benedict (2015), "LLNL's Large Area Projection Micro Stereolithography (LAPuSL0 3D printing device wins tech-transfer awards", available at: http://www.3ders.org/articles/20151002-llnl-3d-printing-device-wins-tech-transfer-award-for-outstanding-technology-development.html (accessed 28 November 2015).

Davis, Wyatt O., Randy Sprague, and Josh Miller. "MEMS-based pico projector display." In Optical MEMs and Nanophotonics, 2008 IEEE/LEOS Internationall Conference on, pp. 31-32. IEEE, 2008.

Sprague, Randy, Mark Champion, Margaret Brown, Dean Brown, Mark Freeman, and Maarten Niesten. "Mobile projectors using scanned beam displays." Mobile Displays: Technology and Applications (2008): 565-588.

Wang, C. C. and Chen, Y. (2010), "Layered depth-normal images: A sparse implicit representation of solid models" arXiv preprint arXiv:1009.0794.

Jacobs, P. F. (1992), Rapid prototyping & manufacturing: fundamentals of stereolithography, Society of Manufacturing Engineers. Dearborn, MI.

Gibson, I., Rosen, D. W. and Stucker, B. (2010). Additive manufacturing technologies, Springer, New York, NY.